

# Recoil Products from $p + {}^{118}\text{Sn}$ and $d + {}^{118}\text{Sn}$ at 3.65 GeV/A

A.R. Balabekyan <sup>1,\*</sup>, A.S. Danagulyan <sup>1</sup>, J.R. Drnoyan <sup>1</sup>, G.H. Hovhannisyan <sup>1</sup>,  
 N.A. Demekhina <sup>2</sup>,  
 J. Adam <sup>3,4</sup>, V.G. Kalinnikov <sup>3</sup>, M.I. Krivopustov <sup>3</sup>, V.S. Pronskikh <sup>3</sup>, V.I. Stegailov <sup>3</sup>,  
 A.A. Solnyshkin <sup>3</sup>, P. Chaloun <sup>3,4</sup>, V.M. Tsoupko-Sitnikov <sup>3</sup>  
 S.G. Mashnik <sup>5</sup>, K.K. Gudima <sup>6</sup>

## Abstract

The recoil properties of the product nuclei from the interaction of 3.65 GeV/nucleon protons and deuterons from the Nuclotron and Synchrophasotron of the Laboratory of High Energies (LHE), Joint Institute for Nuclear Research (JINR) at Dubna with a  ${}^{118}\text{Sn}$  target have been studied using catcher foils. The experimental data were analyzed using the mathematical formalism of the standard two-step vector model. The results for protons are compared with those for deuterons. Our experimental results were compared to three different Los Alamos versions of the Quark-Gluon String Model (LAQGSN). The forward velocity  $v$  and the recoil nuclei kinetic energy increases linearly with increasing mass loss of the target  $\Delta A$ , but seems to change its slope at around  $\Delta A = 60$ . It seems that light- and medium-mass products are produced partly by a fragmentation mechanism.

## 1 Introduction

The investigation of interactions of high-energy particles with complex nuclei by the induced activity method is limited to measurements on the large residual nuclei that remain at the end of reactions. The study of large residual nuclei usually involves measurements of either their excitation functions or their recoil properties.

In order to determine the recoil properties of nuclei “thick-target thick-catcher” experiments are used. In such experiments, the thicknesses of the target and catcher foils are larger than the longest recoil range. The quantities measured are the fractions  $F$  and  $B$  of product nuclei that recoil out of the target foil into the forward and backward directions, respectively.

The results of the experiment are usually proceeded by the standard two-step vector representation [1]–[3]. The following assumptions are made in this model:

(1) In the first step, the incident particle interacts with the target nucleus to form an excited nucleus with velocity  $v$ , momentum  $P$ , and excitation energy  $E^*$ .

(2) In the second step, the excited nucleus loses mass and excitation energy to form the final recoiling nucleus with an additional velocity  $V$ , which in general will have a distribution of values and directions.

Usually, additional assumptions are made in most experiments:

(a) The quantities  $v$  and  $P$  in the first step are constant [4] and lie in the forward direction.

---

<sup>1</sup>Yerevan State University, Armenia

<sup>2</sup>Yerevan Physics Institute, Armenia

<sup>3</sup>JINR, Dubna, Russia

<sup>4</sup>INF AS Řež, Czech Republic

<sup>5</sup>Los Alamos National Laboratory, Los Alamos, USA

<sup>6</sup>Institute of Applied Physics, Academy of Science of Moldova, Chişinău

(b) The velocity in the second step is isotropic.

The results of the recoil experiments depend on the range-energy relation of the recoiling nuclei. It is convenient to express this relation as [2]:

$$R = kV^n, \quad (1)$$

where  $R$  is the mean range (corresponding to  $V$ ) of the recoil in the target material,  $k$  and  $n$  are constants and can be evaluated from tables of ranges of nuclei recoiling into various materials [5]. The following relations are used for the forward and backward fractions:

$$FW = \frac{1}{4}R[1 + \frac{2}{3}(n+2)\eta + \frac{1}{4}(n+1)^2\eta^2]; \quad BW = \frac{1}{4}R[1 - \frac{2}{3}(n+2)\eta + \frac{1}{4}(n+1)^2\eta^2] \quad (2)$$

where  $\eta = v/V$  and  $W$  is the target thickness in  $mg/cm^2$ .

The reaction product mean ranges ( $R$ ) and the velocities transferred to residuals on the first ( $v$ ) and second ( $V$ ) steps of reaction are calculated using the following expressions [2]:

$$F/B = \frac{1 + \frac{2}{3}(n+2)\eta + \frac{1}{4}(n+1)^2\eta^2}{1 - \frac{2}{3}(n+2)\eta + \frac{1}{4}(n+1)^2\eta^2}; \quad R = 2W(F+B)/(1 + \frac{1}{4}(n+1)^2\eta^2) \quad (3)$$

The recoil properties of non-fission reactions induced by protons with energy 1 GeV and above were analyzed with the two-vector model in Ref. [6]. Systematic deviations of the resulting parameters were attributed to the presence of fragmentation. The kinematic properties of radionuclides formed in photospallation reactions on complex nuclei at intermediate energy and a comparison with proton-nuclear reactions were made in Ref. [7]. We studied the recoil properties of nuclei produced in the photospallation of  $^{65}\text{Cu}$  in Ref. [8]. The purpose of the present work is to investigate the kinematic properties of product nuclei formed in the target  $^{118}\text{Sn}$  bombarded with 3.65 GeV/nucleon protons and deuterons using catcher foils.

## 2 Experimental setup and results

Targets of enriched tin isotope  $^{118}\text{Sn}$  were irradiated at the Nuclotron and Synchrophasotron of the LHE, JINR by proton and deuteron beams with energies of 3.65 GeV/nucleon. Irradiations were of 6.42 hour for the proton beam and 1.083 hour for the deuteron beam. The deuteron beam had an elliptic form with axes of 3 and 2 cm. The proton beam had round form with a diameter of 2 cm. For beam monitoring, we employ the reactions  $^{27}\text{Al}(d, 3p2n)^{24}\text{Na}$  and  $^{27}\text{Al}(p, 3pn)^{24}\text{Na}$  whose cross sections are taken as of  $14.2 \pm 0.2\text{mb}$  [9] and  $10.6 \pm 0.8\text{mb}$  [10], respectively. From the monitoring reactions the following beam intensities were obtained:  $0.768 \times 10^{13}$  d/hour and  $0.114 \times 10^{13}$  p/hour. The total beam fluences were  $3.21 \times 10^{13}$  protons and  $2 \times 10^{13}$  deuterons.

The target consisted of a high-purity target metal foil of size 20x20 mm<sup>2</sup> sandwiched exactly by one pair of Mylar foils of the same size, which collected the recoil nuclei in the forward or backward directions with respect to the beam. The enrichment of the target was 98.7 %, the thickness of each target foil was 66.7  $mg/cm^2$  and the number of target piles was 15. The whole stack, together with an Al beam-monitor foil of 140  $mg/cm^2$  thickness was mounted on a target holder and irradiated in air.

After irradiation the target foils and all of the forward and backward catcher foils from one target pile were collected separately, and assayed for radioactivities nondestructively with

high-purity Ge detectors at LNP, JINR for one year. The radioactive nuclei were identified by characteristic  $\gamma$  lines and by their half-lives. The spectra were evaluated with the code package DEIMOS32 [11].

The kinematic characteristics of thirty product nuclei were obtained for deuteron- and proton-induced reactions. The relative quantities of the forward- and backward-emitted nuclei (relative to the beam direction) were calculated from relations:

$$F = N_F / (N_t + N_F + N_B); \quad B = N_B / (N_t + N_F + N_B) \quad (4)$$

where  $N_F$ ,  $N_B$ ,  $N_t$  are the numbers of nuclei emitted in forward and backward catchers and formed in target foils, respectively. The recoil parameters obtained in these experiments are the forward-to-backward ratio,  $F/B$ , and the mean range,  $2W(F + B)$ . [The mean range of the recoils is somewhat smaller than  $2W(F + B)$ , but it is conventional to refer to the latter quantity as range]. The mathematical formalism of the standard two-step vector model [2] was used to proceed the experimental results. The parameters  $k$  and  $n$  in equation (1) are obtained by fitting the range dependence on energy of accelerated ions within the region from 0.025 to 5 MeV/nucleon [12]. It is possible to calculate  $\eta$  and  $v$  from the equation (3), knowing the  $F/B$  ratio of the experiment.

Our experimental results are shown in Tables 1 and 2. We note that uncertainties concerning definite quantities in our tables are not listed to keep the tables concise. These uncertainties are about 10–15%. As is seen from the tables, the kinetic energies of product nuclei from proton-induced reactions are higher than are the ones induced by deuterons. Probably, protons are more effective agents of linear momentum transfer on a per-nucleon basis when compared with deuterons [13, 14].

As shown in Fig. 1, the ratios  $F/B$  for both proton- and deuteron-induced reactions are of the order of  $\sim 3 - 4$  for heavy product nuclei and decrease to about  $\sim 2$  for light residuals. Such a dependence could be explained by different mechanisms for the production of nuclei in different mass regions. Light nuclei may be produced by multifragmentation and evaporation that lead to an isotropic distribution in the frame of excited residual nuclei, while heavy nuclei are produced mainly via the spallation mechanism, with its products more in the forward direction. Some of our recent studies [15, 16] point to the multifragmentation mechanism in the formation of product nuclei with light and medium mass numbers.

Our experimental results are compared with theoretical calculations by the LAQGSM03.01 [17], LAQGSM03.S1 [18], and LAQGSM03.G1 [18] models.

LAQGSM03.01 [17] is the latest modification of the Los Alamos version of the Quark-Gluon String Model [19], which in its turn is an improvement of the Quark-Gluon String Model [20]. It describes reactions induced by both particles and nuclei as a three-stage process: IntraNuclear Cascade (INC), followed by preequilibrium emission of particles during the equilibration of the excited residual nuclei formed during the INC, followed by evaporation of particles from or fission of the compound nuclei. The INC stage of reactions is described with a recently improved version [17] of the time-depending intranuclear cascade model developed initially at Dubna, often referred in the literature simply as the **D**ubna **I**ntranuclear **C**ascade **M**odel, DCM (see [21] and references therein). The preequilibrium part of reactions is described with an improved version [22] of the Modified Exciton Model (MEM) from the Cascade-Exciton Model, CEM [23]. The evaporation and fission stages of reactions are calculated with an updated and improved version of the Generalized Evaporation Model code GEM2 by Furihata [24], which considers evaporation of up to 66 types of different particles and light fragments (up to  $^{28}\text{Mg}$ ). If the excited residual nucleus produced after the INC has a mass number  $A \leq 11$ , LAQGSM03.01

uses a recently updated and improved version of the Fermi Break-up model (in comparison with the version described in [20]) to calculate its decay instead of considering a preequilibrium stage followed by evaporation from compound nuclei, as described above. LAQGSM03.01 considers also coalescence of complex particles up to  ${}^4\text{He}$  from energetic nucleons emitted during the INC, using an updated coalescence model in comparison with the version described in [21].

LAQGSM03.S1 [18] is exactly the same as LAQGSM03.01, but considers also multifragmentation of excited nuclei produced after the preequilibrium stage of reactions, when their excitation energy is above  $2A$  MeV, using the Statistical Multifragmentation Model (SMM) by Botvina et al. [25] (the “S” in the extension of LAQGSM03.S1 stands for SMM).

LAQGSM03.G1 [18] is exactly the same as LAQGSM03.01, but uses the fission-like binary-decay model GEMINI of Charity et al. [26], which considers evaporation of all possible fragments, instead of using the GEM2 model [24] (the “G” stands for GEMINI).

As can be seen from Fig. 1, there is some disagreement between experimental data and theoretical results by all three versions of LAQGSM considered here. In making such a comparison, we first recognize that the experiment and the calculations differ in that: 1) the experimental data were extracted assuming the “two-step vector model” [1]–[3], while the LAQGSM calculations were done without the assumptions of this model; 2) the measurements were performed on foils (thick targets), while the calculations were done for interactions of protons/deuterons with nuclei (thin targets). These differences must be considered before assessing possible deficiencies in the models.

It is interesting to note that the measured forward velocity  $v$  increases practically linearly with the increase of  $\Delta A$  ( $\Delta A = A_{\text{targ}} - A_{\text{res}}$ , where  $A_{\text{targ}}$  is the mass number of target and  $A_{\text{res}}$  is the mass number of product nuclei), but seems to change its slope at around  $\Delta A = 60$ . Comparison of these results with theoretical calculations shows that this is due to different mechanisms for the production of the measured nuclei (Fig. 2).

Fig. 3 shows the dependence of the fragment kinetic energy,  $T_{\text{kin}}$ , on the fractional mass loss  $\Delta A/A$ . Cumming and Bächmann [27] and Winsberg [3] have shown that  $T_{\text{kin}}$  should increase linearly with  $\Delta A/A$  for reactions in which the velocity of the product is due to the vectorial addition of the randomly directed recoil velocities resulting from particle emission. For comparison, Fig. 3 shows also data measured for a Ag target by Porile et al. (see Table II in [6] and references therein). One can see that the Ag results agree well with our current  ${}^{118}\text{Sn}$  data.

The deviation from a linear trend seen in Fig. 3 for large fractional mass losses probably indicates a change in mechanism of the production of light nuclides. The formation of light fragments from highly-excited nuclei is of a permanent interest in the literature and usually considers a multi-body breakup [28]. One possible mechanism for such a process would be a simultaneous clustering of nucleons into fragments near the liquid-gas critical point [25]. This process is essentially different from the sequential evaporation process by which deep spallation products are formed. It appears that the mean kinetic energies of the products provide a qualitative method for distinguishing between these two mechanisms [29].

As one can see from Fig. 3, the results by LAQGSM03.S1, which considers multifragmentation [25] of excited nuclei when their excitation energy is above 2 MeV/nucleon, overestimate significantly the values of the measured mean kinetic energies of light products. This could be an indication that multifragmentation becomes important only at higher excitation energies, 4–5 MeV/nucleon instead of 2 MeV/nucleon as considered by LAQGSM03.S1, in complete agreement with the very recent ISiS measurements [30].

The evaluated “experimental” excitation energies of residual nuclei produced after the first,

cascade stage of reactions are shown in the last column of Tables 1 and 2. The relation between the excitation energy ( $E^*$ ) and  $v$  may be estimated as [32]:

$$E^* = 3.253 * 10^{-2} k' A_T v [T_p / (T_p + 2)]^{0.5}, \quad (5)$$

where  $E^*$  and the bombarding energy  $T_p$  are expressed in terms of  $m_p c^2$ .  $A_T$  is the target mass in  $amu$  and  $v$  is in units of  $(\text{MeV}/amu)^{0.5}$ . Usually, the constant  $k'$  is taken as  $k' = 0.8$ .

As is seen from tables, the excitation energies estimated according to Eq. (5) are higher than the multifragmentation threshold  $E_{th} = 2 - 4 \text{ MeV/nucleon}$  ( $E_{tot} = 216 - 424 \text{ MeV}$ ) [31] for the light and medium products. This could be an indication that light and medium fragments are produced not only via the evaporation mechanism but also via multifragmentation.

## Acknowledgments

The authors would like to express their gratitude to the operating personnel of the JINR Nuclotron and Synchrophasotron for providing good beam parameters and to thank Dr. A.J. Sierk of LANL for a most useful critical reading.

This work was supported partially by the US DOE.

## References

- [1] N. Sugarman, M. Campos, K. Wielgoz, Phys. Rev. 101 (1956) 388.
- [2] L. Winsberg, Nucl. Instrum. Methods 150 (1978) 465.
- [3] L. Winsberg, Phys. Rev. C 22 (1980) 2116.
- [4] R.G. Kortelling, C.R. Toren, E.K. Hyde, Phys. Rev. C 7 (1973) 1611.
- [5] L. Winsberg, At. Data Nucl. Data Tables 20 (1977) 389.
- [6] L. Winsberg, Phys. Rev. C 22 (1980) 2123.
- [7] H. Haba, H. Matsumura, K. Sakamoto, Y. Oura, S. Shibata, M. Furukawa, I. Fujiwara, Radiochim. Acta 88 (2000) 375.
- [8] A.A. Arakelyan, A.R. Balabekyan, A.S. Danagulyan, A.G. Khudaverdyan, Nucl. Phys. A534 (1991) 535.
- [9] Ts. Damdinsuren, V.I. Iluschenko, P. Kozma, B. Tumendemberel, D. Chultem, Yad. Fiz. 52 (1990) 330 [Sov. J. Nuc. Phys. 52 (1990) 209].
- [10] R. Michel, M. Gloris, H.-J. Lange, I. Leya, M. Lüpke, U. Herpers, B. Dittrich-Hannen, R. Rösel, Th. Scielke, D. Filges, P. Dragovitsch, M. Suter, H.-J. Hoffmann, W. Wölfli, P.W. Kubik, H. Bauer, R. Wieler, Nucl. Instrum. Methods B 103 (1995) 183.
- [11] J. Frána, J. Radioanal. Nucl. Chem. 257 (2003) 583.
- [12] L.C. Northcliffe, R.F. Schilling, Nucl. Data A 7 (1970) 233.

- [13] F. Saint Laurent, M. Conjeaud, R. Dayras, S. Harar, H. Oeschler, C. Volant, Phys. Lett. B 110 (1982) 372; F. Saint-Laurent, M. Conjeaud, R. Dayras, S. Harar, H. Oeschler, C. Volant, Nucl. Phys. A 422 (1984) 307.
- [14] M. Bronikowski, N.T. Porile, Phys. Rev. C 44 (1991) 1661.
- [15] V. Aleksandryan, J. Adam, A. Balabekyan, A.S. Danagulyan, V.G. Kalinnikov, G. Musulmanbekov, V.K. Rodionov, V.I. Stegailov, J. Frana, Nucl. Phys. A 674 (2000) 539.
- [16] A.R. Balabekyan, A.S. Danagulyan, J.R. Drnoyan, N.A. Demekhina, J. Adam, V.G. Kalinnikov, G. Musulmanbekov, Nucl. Phys. A 735 (2004) 267.
- [17] S.G. Mashnik, K.K. Gudima, M.I. Baznat, A.J. Sierk, R.A. Prael, N.V. Mokhov, LANL Report, LA-UR-05-2686, Los-Alamos (2005).
- [18] S.G. Mashnik, K.K. Gudima, M.I. Baznat, A.J. Sierk, R.A. Prael, N.V. Mokhov, LANL Report, LA-UR-06-1764, Los-Alamos (2006).
- [19] K.K. Gudima, S.G. Mashnik, A.J. Sierk, LANL Report LA-UR-01-6804, Los Alamos (2001), <http://lib-www.lanl.gov/la-pubs/00818645.pdf>.
- [20] N.S. Amelin, K.K. Gudima, V.D. Toneev, Yad. Fiz. 51 (1990) 512 [Sov. J. Nucl. Phys. 51 (1990) 327]; Yad. Fiz. 51 (1990) 1730 [Sov. J. Nucl. Phys. 51 (1990) 1093]; Yad. Fiz. 52 (1990) 272 [Sov. J. Nucl. Phys. 52 (1990) 172]; N. Amelin, CERN/IT/ASD Report CERN/IT/99/6, Geneva, Switzerland (1999); <http://wwwinfo.cern.ch/asd/geant4/G4UsersDocuments/UsersGuides/PhysicsReferenceManual/html/PhysicsReferenceManual.html>.
- [21] V.D. Toneev, K.K. Gudima, Nucl. Phys. A 400 (1983) 173c.
- [22] S.G. Mashnik, K.K. Gudima, A.J. Sierk, M.I. Baznat, N.V. Mokhov, LANL Report LA-UR-05-7321, Los Alamos (2005); RSICC Code Package PSR-532, <http://www-rsicc.ornl.gov/codes/psr/psr5/psr-532.html> (2006).
- [23] K.K. Gudima, S.G. Mashnik, V.D. Toneev, Nucl. Phys. A 401 (1983) 329.
- [24] S. Furihata, Nucl. Instrum. Methods B 171 (2000) 252; PhD thesis, Tohoku University, March, 2003.
- [25] J.P. Bondorf, A.S. Botvina, A.S. Iljinov, I.N. Mishustin, K. Sneppen, Phys. Rep. 257 (1995) 133.
- [26] R.J. Charity, M.A. McMahan, G.J. Wozniak, R.J. McDonald, L.G. Moretto, D.G. Sarantites, L.G. Sobotka, G. Guarino, A. Pantaleo, L. Fiore, A. Gobbi, K. D. Hildenbrand, Nucl. Phys. A 483 (1988) 371.
- [27] J.B. Cumming, K. Bächmann, Phys. Rev. C 6 (1972) 1362.
- [28] A.S. Botvina, I.N. Mishustin, Phys. Lett. B 294 (1992) 23.
- [29] C.F. Wang, N.T. Porile, Nucl. Phys. A 468 (1987) 711.

- [30] V.E. Viola, K. Kwiatkowski, L. Beaulieu, D.S. Bracken, H. Breuer, J. Brzychczyk, R.T de Souza, D.S. Ginger, W-c. Hsi, R.G. Korteling, T. Lefort, W.G. Lynch, K.B. Morley, R. Legrain, L. Penkowski, E.C. Pollacco, E. Renshaw, A. Raungma, M.B. Tsang, C. Volant, G. Wang, S.J. Yennello, nucl-ex/0604012.
- [31] A.S. Botvina, I.N. Mishustin, nucl-th/0510081.
- [32] O. Scheidemann, N. Porile, Phys. Rev. C 14 (1976) 1534.

**Table 1.** Kinematic characteristics of product nuclei from deuteron-induced reactions

| Product            | $F/B$ | $\eta$ | $2W(F+B)$ | $T_{kin}$ (MeV) | $v$ (MeV/ $amu$ ) <sup>1/2</sup> | $E^*$ (MeV) |
|--------------------|-------|--------|-----------|-----------------|----------------------------------|-------------|
| <sup>24</sup> Na   | 2.03  | 0.175  | 4.08±0.40 | 15.75± 2.37     | 0.2255                           | 619.62      |
| <sup>28</sup> Mg   | 1.77  | 0.142  | 4.49±0.70 | 19.70± 4.80     | 0.1913                           | 522.36      |
| <sup>42</sup> K    | 2.36  | 0.212  | 2.49±0.60 | 12.07± 5.11     | 0.1861                           | 496.32      |
| <sup>43</sup> K    | 2.73  | 0.246  | 1.93±0.35 | 7.54± 2.42      | 0.1680                           | 449.30      |
| <sup>44m</sup> Sc  | 2.00  | 0.172  | 2.49±0.58 | 12.21±4.63      | 0.1457                           | 394.77      |
| <sup>52g</sup> Mn  | 1.97  | 0.168  | 0.94±0.21 | 2.86 ±1.03      | 0.0678                           | 172.55      |
| <sup>56</sup> Mn   | 2.39  | 0.215  | 1.67±0.61 | 6.91 ±4.06      | 0.1212                           | 329.11      |
| <sup>67</sup> Ga   | 2.18  | 0.193  | 1.51±0.44 | 6.89 ±3.21      | 0.0996                           | 270.13      |
| <sup>73</sup> Se   | 3.08  | 0.274  | 0.72±0.16 | 2.25± 0.83      | 0.0769                           | 210.08      |
| <sup>75</sup> Br   | 3.02  | 0.269  | 0.94±0.28 | 3.46± 1.70      | 0.0927                           | 252.67      |
| <sup>77</sup> Br   | 1.97  | 0.167  | 1.41±0.39 | 6.51± 2.88      | 0.0785                           | 212.61      |
| <sup>81</sup> Rb   | 4.09  | 0.338  | 1.14±0.14 | 4.85± 0.98      | 0.1318                           | 361.96      |
| <sup>71</sup> As   | 2.84  | 0.255  | 1.45±0.27 | 6.74± 2.03      | 0.1261                           | 343.88      |
| <sup>83</sup> Sr   | 3.39  | 0.296  | 1.11±0.21 | 4.73± 1.45      | 0.1130                           | 309.10      |
| <sup>85</sup> Y    | 3.51  | 0.304  | 0.89±0.12 | 3.35± 0.72      | 0.0963                           | 263.75      |
| <sup>86m</sup> Y   | 3.09  | 0.275  | 0.97±0.13 | 3.88± 0.82      | 0.0934                           | 254.93      |
| <sup>87m</sup> Y   | 3.44  | 0.299  | 0.97±0.17 | 3.88± 1.12      | 0.1010                           | 276.46      |
| <sup>86</sup> Zr   | 4.78  | 0.372  | 0.78±0.11 | 2.78± 0.66      | 0.1061                           | 292.67      |
| <sup>89</sup> Zr   | 2.96  | 0.265  | 0.88±0.16 | 3.33±0.97       | 0.0821                           | 224.13      |
| <sup>90</sup> Mo   | 2.39  | 0.214  | 0.84±0.17 | 3.26±1.08       | 0.0657                           | 178.49      |
| <sup>93m</sup> Mo  | 2.07  | 0.179  | 0.52±0.07 | 1.46± 0.33      | 0.0362                           | 98.25       |
| <sup>90</sup> Nb   | 3.28  | 0.288  | 0.45±0.09 | 2.38± 0.48      | 0.0515                           | 140.56      |
| <sup>94</sup> Tc   | 3.12  | 0.277  | 0.36±0.09 | 0.86± 0.34      | 0.0423                           | 115.53      |
| <sup>95</sup> Tc   | 3.82  | 0.323  | 0.54±0.08 | 1.61± 0.39      | 0.0669                           | 183.76      |
| <sup>96</sup> Tc   | 2.06  | 0.179  | 0.36±0.06 | 0.85± 0.21      | 0.0270                           | 73.29       |
| <sup>97</sup> Ru   | 3.64  | 0.312  | 0.66±0.16 | 2.28± 0.89      | 0.0764                           | 209.48      |
| <sup>99m</sup> Rh  | 3.56  | 0.307  | 0.45±0.07 | 1.27± 0.33      | 0.0555                           | 152.21      |
| <sup>104</sup> Ag  | 4.46  | 0.357  | 0.23±0.05 | 0.45± 0.14      | 0.0374                           | 103.03      |
| <sup>109</sup> In  | 3.24  | 0.286  | 0.26±0.04 | 0.58± 0.14      | 0.0332                           | 90.91       |
| <sup>110</sup> Sn  | 2.00  | 0.180  | 0.21±0.05 | 0.41± 0.16      | 0.0168                           | 45.73       |
| <sup>111</sup> In  | 2.33  | 0.210  | 0.16±0.04 | 0.26± 0.11      | 0.0161                           | 43.80       |
| <sup>117m</sup> Sn | 2.11  | 0.180  | 0.25±0.05 | 0.56± 0.18      | 0.0064                           | 56.20       |



**Table 2.** Kinematic characteristics of product nuclei from proton-induced reactions

| Product            | $F/B$ | $\eta$ | $2W(F+B)$  | $T_{kin}$ (MeV) | $v$ (MeV/amu) <sup>1/2</sup> | $E^*$ (MeV) |
|--------------------|-------|--------|------------|-----------------|------------------------------|-------------|
| <sup>24</sup> Na   | 1.95  | 0.165  | 5.37± 0.35 | 23.91± 2.36     | 0.2628                       | 583.06      |
| <sup>28</sup> Mg   | 2.03  | 0.175  | 4.61± 0.30 | 20.54± 2.11     | 0.2399                       | 530.01      |
| <sup>42</sup> K    | 2.15  | 0.189  | 3.12± 0.20 | 17.88± 2.04     | 0.2023                       | 435.23      |
| <sup>43</sup> K    | 2.19  | 0.194  | 2.37± 0.14 | 10.83± 1.16     | 0.1595                       | 343.19      |
| <sup>44m</sup> Sc  | 2.50  | 0.225  | 2.83± 0.18 | 14.97± 1.57     | 0.2111                       | 463.51      |
| <sup>46</sup> Sc   | 1.94  | 0.165  | 2.94± 0.20 | 15.60± 1.68     | 0.1547                       | 338.71      |
| <sup>48</sup> Sc   | 2.08  | 0.181  | 2.55± 0.34 | 12.07± 2.60     | 0.1467                       | 321.13      |
| <sup>48</sup> V    | 2.21  | 0.196  | 2.56± 0.19 | 13.67± 1.67     | 0.1687                       | 369.73      |
| <sup>52g</sup> Mn  | 2.21  | 0.196  | 2.09± 0.14 | 10.43± 1.09     | 0.1415                       | 310.03      |
| <sup>58</sup> Co   | 3.21  | 0.284  | 2.38± 0.18 | 12.66± 1.54     | 0.2122                       | 467.95      |
| <sup>67</sup> Ga   | 2.72  | 0.245  | 1.66± 0.11 | 8.04± 0.84      | 0.1362                       | 299.48      |
| <sup>71</sup> As   | 3.83  | 0.324  | 1.54± 0.10 | 7.39± 0.79      | 0.1665                       | 368.74      |
| <sup>73</sup> Se   | 3.96  | 0.331  | 0.97± 0.06 | 3.62± 0.37      | 0.1174                       | 260.25      |
| <sup>75</sup> Se   | 5.17  | 0.389  | 0.98± 0.02 | 3.77± 0.15      | 0.1378                       | 307.88      |
| <sup>77</sup> Br   | 3.23  | 0.285  | 0.94± 0.06 | 3.37± 0.35      | 0.0954                       | 210.39      |
| <sup>81</sup> Rb   | 4.48  | 0.358  | 1.30± 0.07 | 5.99± 0.56      | 0.1547                       | 344.22      |
| <sup>82</sup> Rb   | 3.68  | 0.314  | 0.73± 0.05 | 2.39± 0.25      | 0.0858                       | 189.87      |
| <sup>83</sup> Sr   | 3.32  | 0.291  | 1.22± 0.08 | 5.51± 0.58      | 0.1199                       | 264.95      |
| <sup>85</sup> Y    | 3.97  | 0.331  | 1.00± 0.07 | 3.99± 0.42      | 0.1143                       | 253.54      |
| <sup>86m</sup> Y   | 4.7   | 0.369  | 1.21± 0.08 | 5.51± 0.58      | 0.1478                       | 329.47      |
| <sup>86</sup> Zr   | 3.83  | 0.324  | 0.75± 0.05 | 4.88± 0.43      | 0.1179                       | 272.26      |
| <sup>89</sup> Zr   | 3.82  | 0.323  | 1.04± 0.07 | 4.36± 0.46      | 0.1138                       | 252.26      |
| <sup>90</sup> Mo   | 4.30  | 0.349  | 1.19± 0.08 | 5.74± 0.60      | 0.1401                       | 311.45      |
| <sup>90</sup> Nb   | 4.03  | 0.335  | 0.70± 0.05 | 2.37± 0.25      | 0.0863                       | 191.72      |
| <sup>93m</sup> Mo  | 3.74  | 0.318  | 0.68± 0.05 | 2.27± 0.25      | 0.0792                       | 175.55      |
| <sup>94</sup> Tc   | 3.91  | 0.328  | 0.51± 0.03 | 1.49± 0.16      | 0.0656                       | 145.55      |
| <sup>95</sup> Tc   | 3.59  | 0.309  | 0.65± 0.04 | 2.12± 0.22      | 0.0740                       | 163.99      |
| <sup>96</sup> Tc   | 2.93  | 0.262  | 0.43± 0.04 | 1.12± 0.15      | 0.0453                       | 100.00      |
| <sup>97</sup> Ru   | 3.86  | 0.326  | 0.53± 0.03 | 1.60± 0.17      | 0.0666                       | 147.87      |
| <sup>99m</sup> Rh  | 4.23  | 0.346  | 0.43± 0.03 | 1.18± 0.12      | 0.0599                       | 133.43      |
| <sup>104</sup> Ag  | 4.00  | 0.333  | 0.25± 0.02 | 0.50± 0.05      | 0.0369                       | 81.99       |
| <sup>109</sup> In  | 3.94  | 0.330  | 0.22± 0.01 | 0.42± 0.04      | 0.0325                       | 72.33       |
| <sup>110</sup> Sn  | 3.81  | 0.323  | 0.18± 0.01 | 0.33± 0.03      | 0.0282                       | 62.81       |
| <sup>111</sup> In  | 3.27  | 0.288  | 0.12± 0.01 | 0.16± 0.02      | 0.0177                       | 39.25       |
| <sup>117m</sup> Sn | 3.27  | 0.288  | 0.08± 0.01 | 0.08± 0.02      | 0.0124                       | 27.54       |

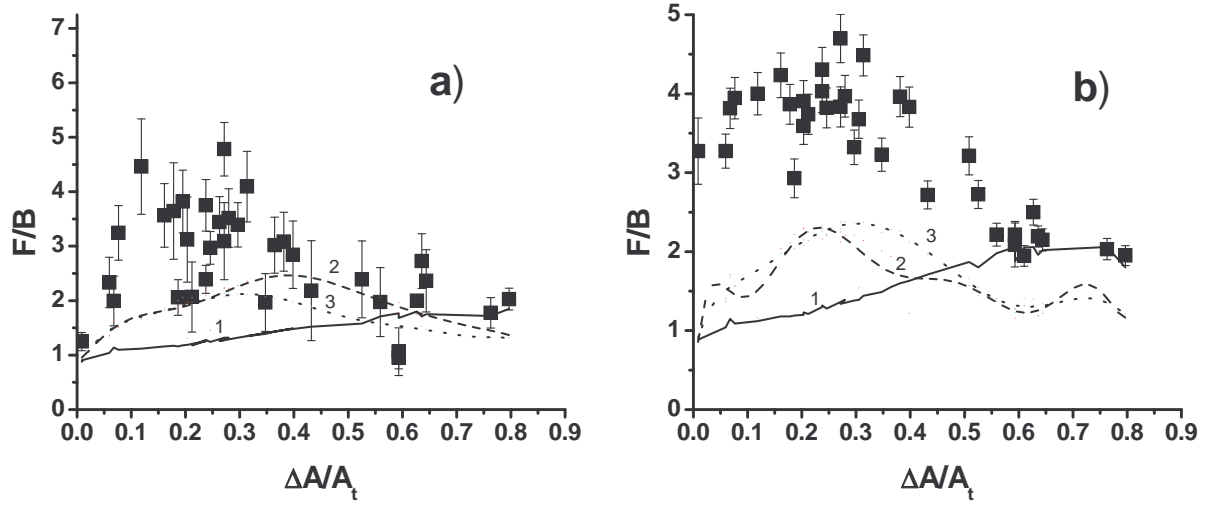


Figure 1:  $F/B$  versus the fractional mass losses  $\Delta A/A_t$ : a) for deuteron-induced reactions b) for proton-induced reactions. Solid lines (1) show calculations by LAQGSM03.01, dashed lines (2) by LAQGSM03.S1, and dotted lines (3) by LAQGSM03.G1.

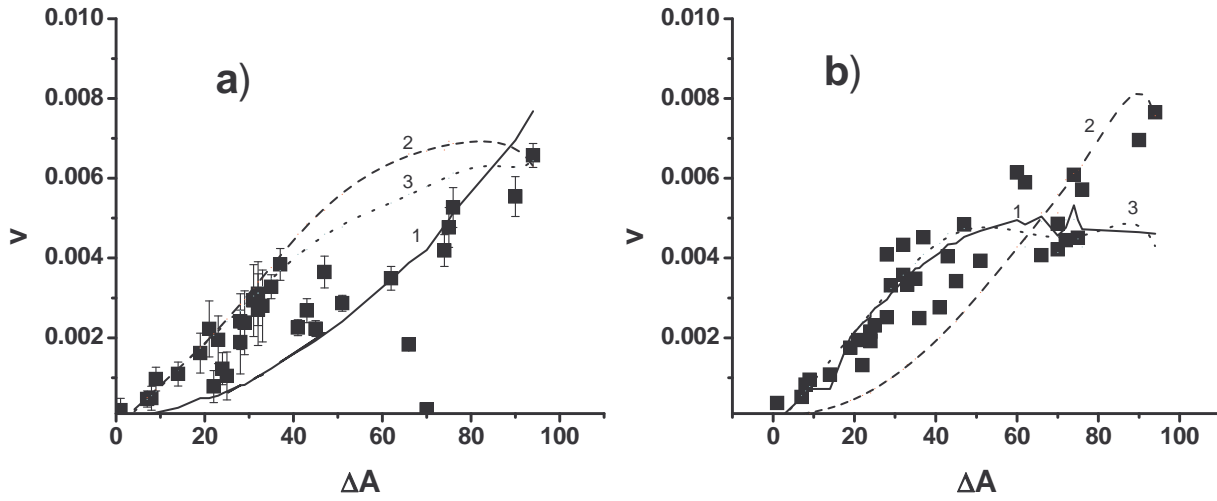


Figure 2: Dependence of forward velocity on the number of emitted nucleons: a) for deuteron-induced reactions b) for proton-induced reactions. Solid lines (1) show calculations by LAQGSM03.01, dashed lines (2) by LAQGSM03.S1, and dotted lines (3) by LAQGSM03.G1.

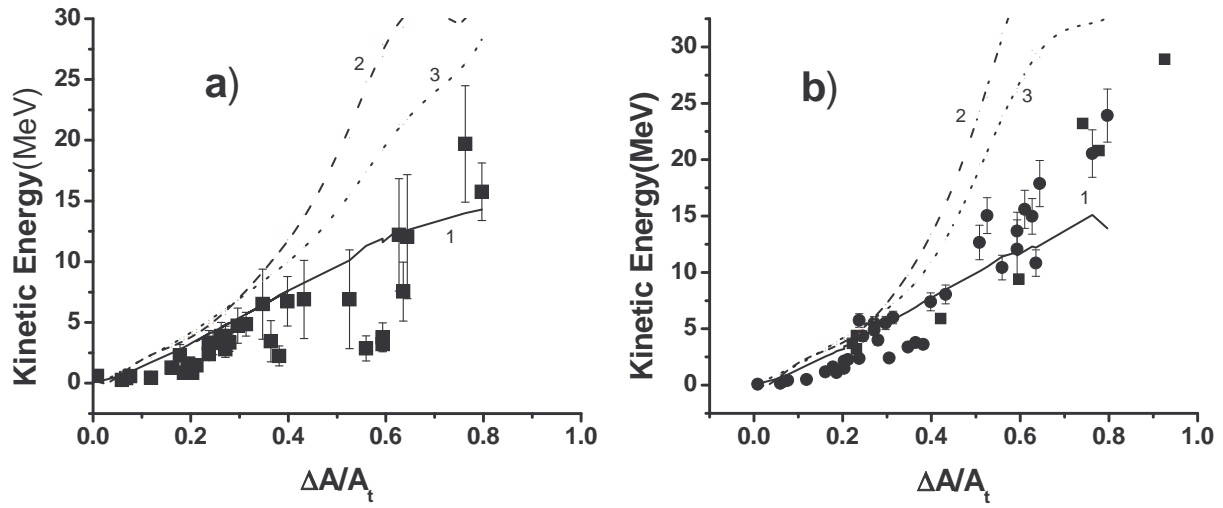


Figure 3: Dependence of the kinetic energy of the product nuclei on the fractional mass losses  $\Delta A/A_t$ : a) for deuteron-induced reactions b) for the proton-induced reactions (●). For comparison, ■ show experimental results for the Ag target tabulated in Ref. [6]. Solid lines (1) show calculations by LAQGSM03.01, dashed lines (2) by LAQGSM03.S1, and dotted lines (3) by LAQGSM03.G1.